Proceedings of the 4th International Conference on Recent Innovation in Engineering
ICRIE 2023, University of Duhok, College of Engineering, 13th – 14th September 2023
(Special issue for Passer journal of basic and applied sciences)
Paper No. 23

Analytical and numerical modeling of plain concrete's post-cracking behavior using a trilinear softening curve

Ghoson DANHASH[1,*], Mais GHASSOUN[2], Mayada KOUSA [3], and George WARDEH[4]

[1]Al-Baath University &Wadi International University/ Syria.
Phone number +963933874237.E-mail:ghosoun.d@gmail.com
[2]Wadi International University.
[3]Damascus University / Syria.
[4]Director of Cergy-Pontoise University institute of technology / France.

ABSTRACT

The aim of the present work is to investigate the softening behavior of a notched concrete beam under a three-point bending test analytically, experimentally, and numerically using XFEM in Abaqus. This study presented a trilinear stress-strain softening curve-based analytical model to describe the complete flexural behavior of plain concrete beams. The article also provides the mathematical equations necessary for calculating the force-crack opening displacement during all cracking phases until failure. An inverse analysis of the force-CMOD curves obtained experimentally has optimized the parameters required for the identification of the tensile stress-crack opening relationship.

The ABAQUS environment was used for numerical modeling using the extended finite element method (XFEM), and a good agreement between the experimental and numerical results has been noticed.

KEYWORDS: Plain concrete; cracking; analytical model; trilinear softening; XFEM.

1 INTRODUCTION

The fracture process in quasi-brittle materials like concrete can be modeled using nonlinear mechanics approaches such as the fictitious crack model developed first by Hillerborg et al. [Hillerborg et al. 1976]. Quasi-brittle materials are characterized by the localization of a non-linear zone within a narrow band; this zone is large. In the fictitious crack model, this nonlinear hinge, see Figure 2, is treated as the softening zone, where the material, though cracked, can still transfer stress, while the rest of the beam retains elastic. The tensile stress in the softening zone is described by a softening curve, which is the relationship between the crack opening displacement (w) and the gradual stress drop after the tensile strength. The Fracture Process Zone "FPZ" starts forming after the tensile stress reaches its ultimate value (Ft). wc is the displacement where no stress can be transferred; beyond this value, the real crack propagation can be predicted through an analytical model proposed first by Ulfkjaer [Ulfkjaer et al. 1995]. He supposed the softening curve to be linear, which does not represent the real behavior of concrete. Olesen adopted Ulfkjaer's model, but he considered the softening curve to be bilinear. In preceding works, this model was investigated, and it has been proven that the model gives the maximum numerical force, which is larger than the experimental one by about 20% [Olesen 2001]; [Wittman *et al.* 1988]. Similar observations were found by Ostergaard [Ostergaard *et al.* 2003]. This bilinear softening-based model can't represent the behavior of large beams and concretes with large maximum aggregates [Wittman 1988]. The problems faced in the bilinear softening-based model are caused by the slight drop of the first line in the bilinear curve [Danhash *et al.* 2014 a, b]. This can be solved using multi-linear softening, where a drop can be corrected without a large increase in critical crack opening displacement. In this study, trilinear softening is adopted (Figure1), and the equations of the moment and the rotation for all cracking phases are found depending on the equilibrium principles of the cracked hinge, in which its width equals half of the beam height [Ulfkjaer et al. 1995]. The strain distribution is considered to be linear. In this study, trilinear softening is adopted (Figure1), and the equations of the moment and the rotation for all cracking phases are found depending on the equilibrium principles of the cracked hinge, whose width equals half of the beam height [Ulfkjaer et al. 1995]. The strain distribution is considered to be linear.

It is significantly more difficult to model a fracture that is expanding in FEM because the mesh must be updated constantly to reflect the geometry of the discontinuity as the crack develops. The requirement to construct a conforming mesh is eliminated by the extended finite element method (XFEM).

Belytschko and Black [Belytschko & Black 1996] developed the extended finite element method to account for the presence of discontinuities in the material independent of the initial mesh generation. The XFEM method is a partition of unity-based approach that improves the classical finite element approximation by using the enrichment functions of Babuska and Melenk [Babuska & Melenk 1996]. In the present study, a numerical simulation using XFEM will be verified and compared with the experimental results.

2 THE DESCRIPTION OF THE NEW SUGGESTED MODEL

The failure of a three-point bending beam was modeled by assuming the development of one crack in the midsection of the beam. The main assumptions of the Ulfkjaer model are adopted using trilinear softening instead of linear ones. The complex stress field around the crack is modeled by a simple spring action in an elastic layer around the crack. This layer has a specific width that is proportional to the height of the beam, and studies found that its width equals half of the beam's height [Brinker & Dahl 1989]. The present model uses bending equilibrium, a cracking criterion, the relative stiffness of crack softening, and the local stiffness of the beam to obtain moment-rotation curves. The elastic response of the beam is linear outside the nonlinear hinge. The fictitious crack is initiated at a point when the stress reaches the tensile strength (Ft); the crack forms normally in the direction of the stress. After the crack is initiated, the two parts of the fictitious crack still transfer stress according to the supposed softening curve (trilinear in the present study). When the crack opening displacement (w) reaches a critical value (wc), the stress transfer becomes zero, and a real crack starts to grow. Only bending is supposed to be present in the fracture-process zone. The compression behavior is assumed to be linearly elastic. The constitutive relationship of the midsection is linear before tensile strength is reached; see Figure 1. The relations between stress and crack opening in trilinear softening are given as follows:

$$\begin{cases} \frac{\sigma}{F_t}=1-a_1 w & 0 < w \leq w_1 \\ \frac{\sigma}{F_t}=b_2-a_2 w & w_1 < w \leq w_2 \\ \frac{\sigma}{F_t}=b_3-a_3 w & w_2 < w \leq w_c \end{cases} , \begin{cases} w_1 = \frac{1-b_2}{a_1-a_2} \\ w_2 = \frac{b_2-b_3}{a_2-a_3} \\ w_c = \frac{b_3}{a_3} \end{cases} \quad (1)$$

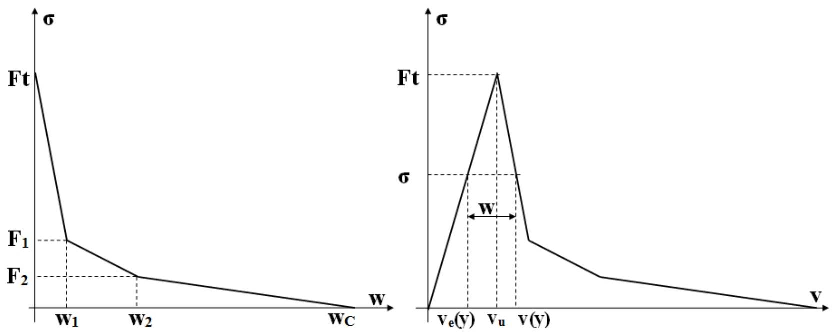

Figure 1. Trilinear softening and the constitutive relation of the midsection

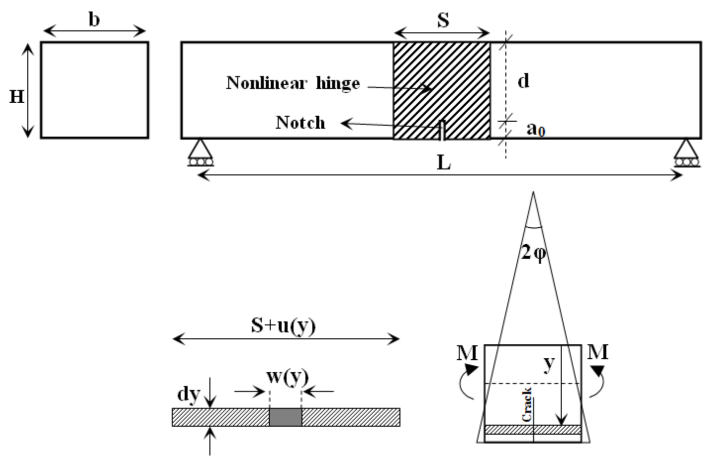

Figure 2. Nonlinear hinge in the notched beam

Points on the crack path pass through five phases, as illustrated in Figure 3. The following normalizations of moment (μ) and rotation (θ) are introduced:

$$\mu = \frac{6\,.M}{b\,.d^2.F_t} \quad (2)$$

$$\theta = \frac{E\,.\,d}{S\,.F_t}\,.\varphi \quad (3)$$

The brittleness of the material is defined by B:

$$B=\frac{Ft.S}{E.w_c} \quad (4)$$

The constants of the model are defined as:

$$\beta_1=\frac{F_t\,.\,S\,.a_1}{E}\,,\ \beta_2=\frac{F_t\,.S\,.\,a_2}{E}\,,\ \beta_3=\frac{F_t\,.S\,.\,a_3}{E} \quad (5)$$

By balancing the sectional stresses with the bending moment M, a relationship between the normalized moment and rotation can be obtained in each phase.

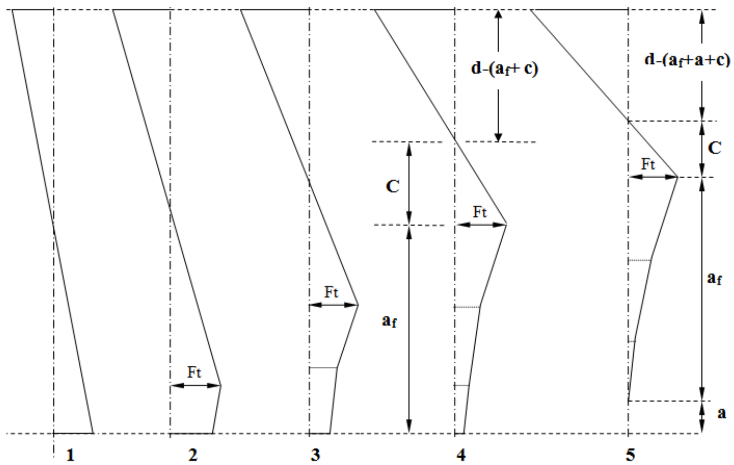

Figure 3. Stress distribution for each phase.

Phase I

This is the elastic phase, where the normalized rotation θ varies between 0 and 1, and the normalized moment μ equals θ.

$\mu = \theta = 1 \ \ , \theta \in [0,1]$ (6)

Phase II

In this phase, the fictitious crack starts to develop after reaching the tensile strength. The equations for this phase are given as follows:

$$\theta_{II}=\frac{1}{2}\left[1+\ \frac{a_f}{C}+\sqrt{1+\left(\ 1+\ \frac{\sigma}{F_t}\right)\frac{a_f}{C}}\right] \quad (7)$$

$$(\frac{a_f}{C})_{II}=\frac{w_1(\ 1\text{-}\ \beta_1)E}{S\ .\ F_t} \quad (8)$$

$$\mu_{II}=4\theta.(1\text{-}\frac{1}{2\theta}(1+\frac{a_f}{c}))^3+\frac{1}{2\theta^2}+\frac{3}{4}\theta^2\frac{a_f}{c}\ (1+\frac{\sigma}{F_t})\left[1+\frac{2}{3}\frac{\frac{1}{2}+\frac{\sigma}{F_t}}{1+\frac{\sigma}{F_t}}\frac{a_f}{c}\right] (9)$$

Where: $\frac{\sigma}{F_t} = \ 1 - \ a_1\ w$

The second phase ends when crack opening w reaches w_1 and stress equals F_2.

Phase III

The stress in the third phase is given as: $\frac{\sigma}{Ft} = b_2 - a_2 w$, and it ends when w=w2, σ=F1.

$$\theta_{III}=\frac{1}{2}\left[1+\frac{a_f}{c}+\sqrt{1+\left(1+\frac{F_1}{F_t}\right)\frac{w_1}{w}\frac{a_f}{c}+\left(\frac{\sigma}{F_t}+\frac{F_1}{F_t}\right)(1\text{-}\frac{w_1}{w})\frac{a_f}{c}}\right] (10)$$

$$\mu_{III} = \mu_1 + \mu_2 + \mu_3 + \mu_4 \ \ (11)$$

$$\mu_1 = 4\ \theta\ \left[1 - \frac{1}{2\theta}\left(1 + \frac{a_f}{c}\right)\right]^3 \quad (12)$$

$$\mu_2 = \frac{1}{2\theta^2} \quad (13)$$

$$\mu_3=\frac{3}{4\ \theta^2}\left(1+\frac{F_1}{F_t}\right)\frac{w_1}{C}\frac{a_f}{C}\left[1+\frac{2}{3}\frac{\frac{1}{2}+\frac{F_1}{F_t}}{1+\frac{F_1}{F_t}}\frac{w_1}{w}\frac{a_f}{C}\right] \quad (14)$$

$$\mu_4=\frac{3}{4\theta^2}\left(1\text{-}\frac{w_1}{w}\right)(\frac{\sigma}{F_t}+\frac{F_1}{F_t})\frac{a_f}{C}\left[1+\frac{w_1}{w}\frac{a_f}{C}+\frac{2}{3}\frac{\frac{1}{2}+\frac{\sigma}{F_t}}{1+\frac{\sigma}{F_t}}(1\text{-}\frac{w_1}{w})\frac{a_f}{C}\right] \quad (15)$$

$$(\frac{a_f}{c})_{III} = \frac{w_2(1-\beta_2)E}{S.F_t} - (1 - b_2) \quad (16)$$

Phase IV

The stress relation is: $\frac{\sigma}{Ft}= b_3\text{-}\ a_3$ w, and the fourth phase ends when w=wc, σ=0. The normalized moment and rotation relations are:

$$\theta=\frac{1}{2}\left\{1+\frac{a_f}{c}+\sqrt{1+\frac{a_f}{c}\left[\left(1+\frac{F_1}{F_t}\right)\frac{w_1}{w}+\left(\frac{F_1}{F_t}+\frac{F_2}{F_t}\right)\left(\frac{w_2}{w}-\frac{w_1}{w}\right)+\left(\frac{\sigma}{F_t}+\frac{F_2}{F_t}\right)(1-\frac{w_2}{w})\right]}\right\} \quad (17)$$

$$\frac{a_f}{c}=\frac{w_c.E}{S.F_t}-1 \quad (18)$$

$$\mu=\mu_1+\mu_2+\mu_3+\mu_4+\mu_5 \quad (19)$$

$$\mu_1=4\,\theta\left[1-\frac{1}{2\,\theta}\left(1+\frac{a_f}{c}\right)\right]^3 \quad (20)$$

$$\mu_2=\frac{1}{2\,\theta^2} \quad (21)$$

$$\mu_3=\frac{3}{4\theta^2}\left(1+\frac{F_1}{F_t}\right)\frac{w_1}{w}a_f\left[1+\frac{2}{3}\frac{\frac{1}{2}+\frac{F_1}{F_t}}{1+\frac{F_1}{F_t}}\frac{w_1}{w}a_f\right] \quad (22)$$

$$\mu_4=\frac{3}{4\theta^2}\frac{a_f}{C}\left(\frac{f_1}{F_t}+\frac{f_2}{F_t}\right)\left(\frac{w_2}{w}-\frac{w_1}{w}\right)\left[1+\frac{w_1}{w}\frac{a_f}{C}+\frac{2}{3}\frac{\frac{1}{2}+\frac{F_2}{F_1}}{1+\frac{F_2}{F_1}}\left(\frac{w_2}{w}-\frac{w_1}{w}\right)\frac{a_f}{C}\right] \quad (23)$$

$$\mu_5=\frac{3}{4\theta^2}\frac{a_f}{C}\left(\frac{\sigma}{F_t}+\frac{F_2}{F_t}\right)(1-\frac{w_2}{w})\left[1+\frac{w_1}{w}\frac{a_f}{C}+\left(\frac{w_2}{w}-\frac{w_1}{w}\right)\frac{a_f}{C}+\frac{2}{3}\frac{\frac{1}{2}+\frac{\sigma}{F_2}}{1+\frac{\sigma}{F_2}}(1-\frac{w_2}{w})\frac{a_f}{C}\right] \quad (24)$$

Phase V:

In the last phase, the crack length has two values: the first is a_f, which is the fictitious crack length, and the other is a, which is the real crack length. This phase ends with failure.

$$\mu=\mu_{cr}\left(\frac{\theta_{cr}}{\theta}\right)^2 \quad (25)$$

Where μ_{cr} is the moment at the end of the fourth phase.

After the μ-θ curve is calculated, the numerical F-CMOD curve can be calculated using the following relations: The bending moment is given by the equation:

$$M=\frac{FL}{4}+\frac{mgL}{8} \quad (26)$$

Where P is the load and m is the weight of the beam in span. From the knowledge of normalized moment μ and using Eq.(A.14) the load can be calculated through the following equation:

$$F=\frac{2\mu F_t d^2 b}{3L}-\frac{1}{2}mg \quad (27)$$

The numerical crack opening should be corrected to match the experimental one, which is measured at a distance (d_0) from the bottom of the beam.

Experimental CMOD has three contributions, as given below:

$$CMOD=COD+CMOD_g+CMOD_e \quad (28)$$

Where COD is related to the crack opening as follows:

$$COD=B.wc.(\frac{w}{wc})^2+\left(2.Ft.\frac{d}{E}\right).\theta.\frac{a_f}{d} \quad (29)$$

$CMOD_g$ is the geometrical opening due to the distance from the notch tip to the measurement point (d_0), and is expressed by the following equation given by Stang [Stang 2000]:

$$CMOD_g=\frac{2(a_0+d_0)d.Ft}{d.E}(\theta-1) \quad (30)$$

$CMOD_e$ is the elastic deformation of the specimen and can be evaluated using the following equation :

$$CMOD_e=\frac{6FLa_0}{E.b.H^2}V \quad (31)$$

V_1 is a geometrical function whose best value is the mean of two expressions given by Stang [Stang 2000]. According to Stang V_1 is given by the following equation:

$$V_1=\left(\frac{a_0+d_0}{a_0}\right)\cdot\left(\begin{array}{c}0.76-2.28.y+\\3.87.y^2-2.04.y^3+\frac{0.66}{(1-y)^2}\end{array}\right) \quad (32)$$

Where: $y=\frac{a_0}{H}$. According to Karihaloo & Nallathambi, V_2 is expressed by the expression [Karihaloo & Nallathambi 1991]:

$$V_2=0.76-2.28.y_1+3.87.y_1^2-2.04.y_1^3+0.66/(1-y_1)^2 \quad (33)$$

With: $y_1=(a_0+H)/(H+d_0)$

Experimental F-CMOD curves are obtained from three-point tests on a notched beam.

3 EXPERIMENTAL PROCEDURES AND SPECIMENS

Materials:

Five different concretes (C1, C2, C3, C4, and C5) were designed according to ACI 911.2-9, prepared using normal Portland cement (fulfilling the ASTM C150 standard), with a maximum aggregate size of 20 [mm], and cured according to ASTM C192.

Mixes from literature:

Some concretes from other research were chosen to enrich the database. The concretes from the literature are: seven different concretes for Zhao [Zhao 2008], one for Roesler [Roesler *et al.* 2007], one for Einsfeld [Einsfeld *et al.* 2006], three for Casuccio [Casuccio et al. 2008], and eight for Zhang [Zhang 2010]. The maximum aggregate size varies between 10 and 80 mm to specify the effect of aggregate size on fracture parameters. Moreover, the paste volume (volume of water plus powder in 1 m^3) for each mix was calculated in order to evaluate its influence on fracture energy. For all mixes, the density of cement was equal to 3100 kg/m3, and the density of fly ash was fixed at 2200 kg/m^3. The compositions of the studied materials are described in Table 1.

Specimens

Beams of different sizes were cast for the bending test, where central notches were milled with different lengths. The ratio a_0/H (notch's length/beam's height) varies from 0.1 to 0.5, so we can specify its effect on fracture parameters. Cylindrical specimens were also cast and tested to determine compressive strength, splitting strength, and elastic modulus. The dimensions of the studied beams are shown in Table 2.

Testing procedure

Three point bending tests were carried out on notched beams, according to RILEM recommendations [3], using testing machines (INSTRON 250 KN for C1, C2, C3, C4, and C5), controlled in displacement mode with a speed rate of 1 mm/sec. The deflection was recorded using an LVDT (Linear Variable Differential Transformer), while the crack opening displacement was recorded by a clip gauge attached to knife edges that was installed at the bottom of the tested beams. Finally, experimental force-CMOD curves are obtained for analysis with the proposed procedure to get fracture parameters.

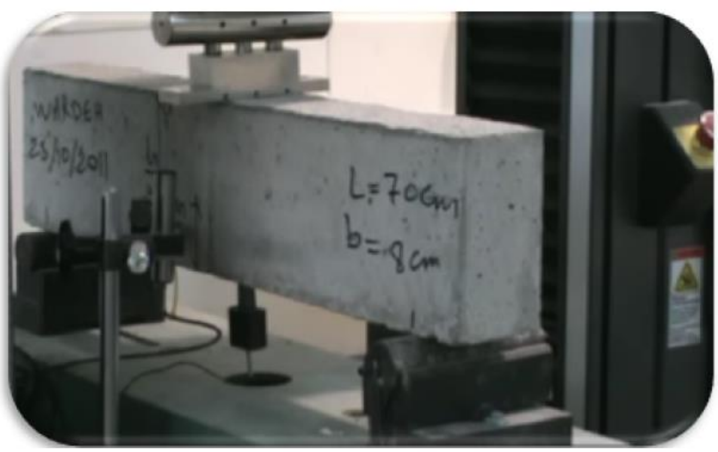

Figure 4. Three-point bending test on a notched beam.

Table 1: Mix proportions of the studied concretes.

Mix	**Cement** **Kg/m^3**	**Gravel** **Kg/m^3**	D_{max} [mm]	**Sand** **Kg/m^3**	**Water** **Kg/m^3**	W.R Kg/m^3	Fly ash	W/ C	A.E %
C1	350	1065	20	970	164	1.89	-	0.47	-
C2	400	1081	20	777	130	1.9	-	0.32	-
C3	400	1081	20	777	160	-	-	0.4	-
C4	400	1045	20	730	200	-	-	0.5	1.5
C5	350	1209	20	586	175	-	-	0.5	1.5
SG1 [Zhao]	196	1090	10	869	140	1.68	84	0.5	1.96
SG3 [Zhao]	240	1154	20	814	135	1.80	60	0.45	1.95
SG4 [Zhao]	309	1145	20	744	135	2.32	77	0.35	2.51
SG5 [Zhao]	420	1121	20	698	140	2.80	47	0.3	2.80
SG6 [Zhao]	168	1287	40	769	120	1.44	72	0.6	1.68
LG1 [Zhao]	159	1496	80	625	102	1.36	68	0.45	1.59
WG1 [Zhao]	159	1065	40	625	102	1.36	68	0.45	1.59
[Roesler]	290	1107	19	718	160	1.68W. R+ 1.65F[1]	88	0.55	0.24
[Einsfeld et al.]	420	992	9.5	860	149	11.5	S.P[2] 11.5	0.31	-
Casuccio G18	263	1080	30	835	184	-	-	0.7	1.5
Casuccio G37	431	1060	30	765	149	4.2	-	0.35	2.5
Casuccio G48	452	960	30	875	155	4.8	-	0.34	3.5
Zhang C40	397	1065	10,16, 20,25	532	205	-	70	0.52	-
Zhang C80	450	1144	10,16, 20,25	572	150	-	SF[3](50)	0.33	-
AE: Air entraining agent. 1: F is high range water reducer. 2: S.P is super plasticizer. 3: SF is silica fume. Fly ash SAI 87%, ASTM C618.									

Table 2: Beams dimensions.

Concrete	**Beam**	Height H [mm]	Width b [mm]	Span L	Notch /height a0/H	Concrete	**Beam**	Height H [mm]	Width B [mm]	**Span** L [mm	Notch /height a0/H
C1	B1	150	80	600	0.33	Zhang	all	100	100	400	0.1
	B2	150	70	600	0.37	Casuccio	all	105	75	400	0.5
	B3	150	68	600	0.37	SG3→6	all	300	120	120	0.4
	B4	150	80	600	0.30	WG1 [Zhao]	B1	250	120	100	0.4
	B5	100	80	600	0.53		B2	300	120	120	0.4
	B6	150	80	600	0.53		B3	400	120	160	0.4
C2	B1	100	100	600	0.25	LG1 [Zhao]	B1	400	240	160	0.4
	B2	100	100	600	0.30		B2	450	240	180	0.4
	B3	100	100	300	0.25		B3	500	240	200	0.4
	B4	150	80	600	0.37		B4	550	240	220	0.4
C3	B1	100	100	600	0.30	SG1 [Zhao]	B1	300	120	120	0.4
	B2	100	100	300	0.25		B2	400	120	160	0.4
	B3	150	80	600	0.37	Einsfeld	B1	76.2	38.1	400	0.5
C4	B1,	100	100	400	0.2		B2	152.4	38.1	400	0.5
	B3,	100	100	400	0.3		B3	304	38.1	400	0.5
	B5,	100	100	400	0.5		B1	150	80	600	0.33

C5	B1,	150	150	600	0.1	Roesler	B4	250	80	100	0.33
	B3,	150	150	600	0.2	C1→C5 Materials of the research					
	B5,	150	150	600	0.3						

4 RESULTS AND DISCUSSION

The parameters of the softening curve for each beam were found by minimizing the differences between the numerical F-CMOD curve and the experimental one using regression. This was made by a procedure developed using MATLAB that gives the numerical F-CMOD curve according to the proposed trilinear-based model. The results are detailed in Table 3.

Table 3. Trilinear softening parameters

Mix	Beam	Material properties			Fmax	GF	Trilinear softening parameters				
		F'c Mpa	E Gpa	Ft Mpa	N	N/m	w1 mm	w2 mm	wc mm	F1 MPa	F2 MPa
C1	B1	33.7	35	3.70	20	198	0.02	0.06	0.14	2.21	1.61
	B2				20	193	0.01	0.04	0.13	2.69	1.93
	B3				20	176	0.03	0.07	0.13	2.11	1.33
	B4				20	198	0.02	0.07	0.15	1.93	1.43
	B5				20	170	0.03	0.07	0.12	1.88	1.17
	B6				20	184	0.01	0.05	0.16	2.58	1.43
C2	B1	50	46	5.15	20	153	0.01	0.04	0.16	2.07	1.30
	B2				20	129	0.01	0.03	0.12	2.09	1.36
	B3				20	158	0.01	0.04	0.12	2.55	1.64
	B4				20	114	0.02	0.05	0.19	2.10	1.45
C3	B1	33	31.1	3.33	20	236	0.04	0.11	0.37	1.35	0.87
	B2				20	241	0.04	0.11	0.39	1.26	0.85
	B3				20	228	0.04	0.13	0.43	1.33	0.67
C4	B1	37	30	3.50	20	181	0.09	0.18	0.37	0.86	1.75
	B2				20	164	0.08	0.17	0.40	0.87	1.63
	B3				20	153	0.07	0.19	0.37	0.79	1.55
	B4				20	173	0.09	0.17	0.37	0.85	1.80
	B5				20	170	0.07	0.19	0.33	0.90	1.79
	B6				20	183	0.09	0.77	0.39	0.85	1.79
C5	B1	28	25	2.70	20	118	0.02	0.05	0.11	0.68	1.35
	B2				20	122	0.02	0.06	0.09	0.60	1.41
	B3				20	119	0.02	0.06	0.09	0.63	1.50
	B4				20	112	0.02	0.06	0.10	0.60	1.37
	B5				20	110	0.02	0.06	0.10	0.57	1.46
	B6				20	181	0.22	0.05	0.11	0.58	1.60
SG1	B1	43.8	31.4	3.73	20	303	0.01	0.12	0.19	1.99	1.02
	B2				20	315	0.04	0.28	0.54	0.86	0.63
SG3	B1	50.9	35.7	3.45	20	248	0.03	0.12	0.27	1.45	1.18
SG4	B1	56.4	35.9	3.67	20	241	0.02	0.13	0.26	1.42	0.91
SG5	B1	50.2	41	3.42	20	221	0.02	0.11	0.23	1.56	1.05
SG6	B1	50.8	38.9	3.45	40	249	0.03	0.17	0.38	1.05	0.82
	B1	40	33.6	3.51	40	176	0.03	0.09	0.27	1.36	0.81

WG1	B2				40	292	0.06	0.17	0.43	1.29	0.72
	B3				40	322	0.06	0.20	0.62	1.22	0.63
LG1	B1	40	33	3.51	80	376	0.07	0.41	0.93	0.68	0.56
	B2				80	381	0.06	0.36	0.77	0.73	0.57
	B3				80	420	0.07	0.41	0.80	0.76	0.56
	B4				80	389	0.10	0.34	0.97	0.76	0.65
Roesler	B1	58.3	32	3.74	20	187	0.03	0.08	0.27	1.41	0.85
	B2				20	204	0.03	0.09	0.28	1.45	0.93
	B3				20	186	0.02	0.07	0.21	1.73	1.08
	B4				20	231	0.03	0.11	0.37	1.42	0.79
	B5				20	163	0.02	0.06	0.20	1.55	0.99
	B6				20	150	0.02	0.07	0.21	1.51	0.82
Eins-field	B1	78	36.2	4.63	20	129	0.01	0.03	0.11	2.07	1.22
	B2				20	152	0.01	0.07	0.12	2.29	0.73
	B3				20	133	0.01	0.07	0.17	1.55	0.71
Casuc-cio	B1	18.1	27.1	3.40	30	101	0.02	0.12	0.21	0.88	0.30
	B2	37.5	33.1	4.10	30	124	0.01	0.07	0.16	1.54	0.68
	B3	48.4	39.9	5.30	30	131	0.01	0.07	0.18	1.45	0.72
Zhang C40	D10	39.55	30	3.20	10	168	0.01	0.10	0.18	0.97	0.30
	D10				10	126	0.00	0.06	0.10	1.08	0.31
	D16	40.05	30	4.55	16	180	0.01	0.10	0.21	1.49	0.60
	D16				16	172	0.02	0.14	0.25	1.43	0.50
	D20	39.23	30	6.19	20	252	0.03	0.24	0.43	2.75	0.94
	D20				20	251	0.04	0.26	0.44	1.67	0.59
	D25	40.07	30	2.87	25	207	0.03	0.25	0.37	0.93	0.24
	D25				25	301	0.03	0.23	0.40	1.73	0.59
Zhang C80	D10	85.2	35	5.79	10	165	0.01	0.07	0.12	2.62	0.96
	D10				10	184	0.01	0.05	0.13	2.73	1.40
	D16	85.42	35	5.33	16	198	0.01	0.07	0.13	2.82	1.21
	D16				16	157	0.01	0.07	0.12	2.41	0.93
	D20	82.29	35	5.45	20	220	0.01	0.08	0.14	2.79	1.09
	D20				20	220	0.01	0.08	0.14	2.79	1.09
	D25	82.28	35	3.84	25	251	0.03	0.19	0.30	1.42	0.39
	D25				25	212	0.02	0.12	0.22	2.07	0.82

Another procedure to get the numerical F-CMOD curve was proposed using a bilinear softening-based analytical model [Karihaloo& Nallathambi 1991], and all experimental results were analyzed through this approach.

The numerical maximum force was plotted versus the experimental one, as shown in Figure 4. The numerical value is close to the experimental one in the trilinear softening-based model, while it is larger for the bilinear one [Karihaloo& Nallathambi 1991].

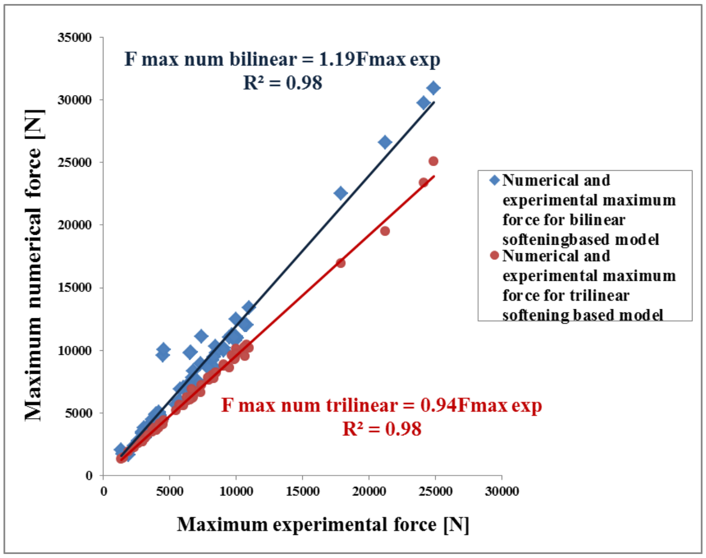

Figure 5. The experimental maximum force versus the numerical one

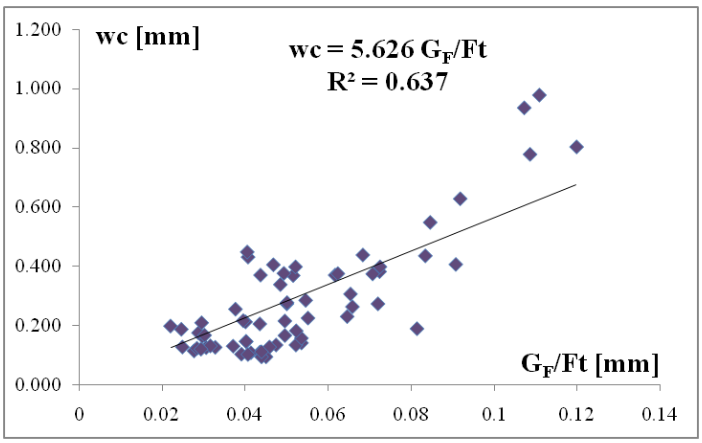

Figure 6. The relation between critical crack opening and fracture energy to the tensile strength ratio

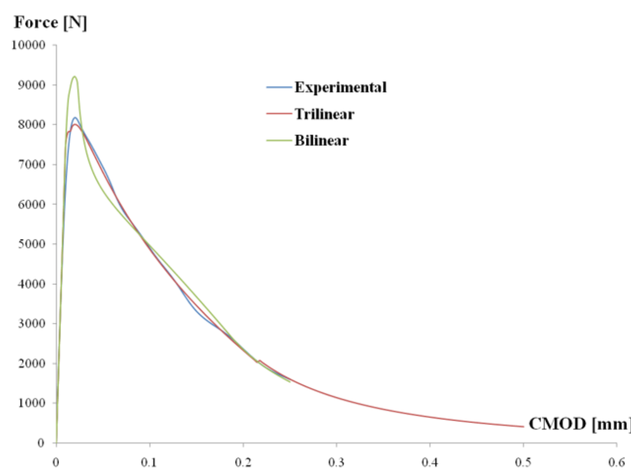

Figure 7. Comparison between the experimental F-CMOD curve and the numerical one calculated from the bilinear and trilinear-based softening models

The mean trilinear curve for all concretes was found depending on wc, Ft and the normalized trilinear curve found is represented in Figure 8.

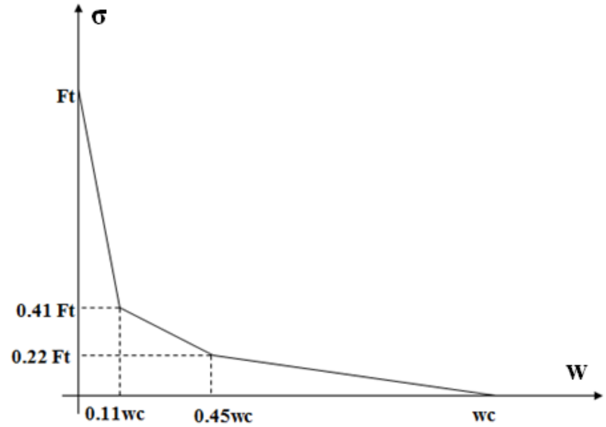

Figure 8. Normalized trilinear softening curve.

5 NUMERICAL SIMULATION:

A three-point bending beam was modeled in ABAQUS using the extended finite element method (XFEM) approach for the C1B1 beam. The beam was modeled using FEM, while the cracking zone was modeled using XFEM. The simplified linear softening equation is utilized, till the fracture begins; after that, the fracture will propagate according to the defined softening. Until the cohesive strength of the cracked element is zero, the cohesive law controls the size of the separation; at this stage, the phantom and real nodes move independently, see Figure 9.

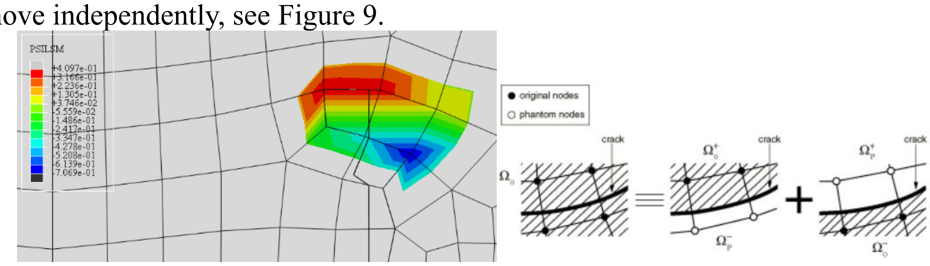

Figure 9. The principle of the phantom node method.

Force – Crack Mouth Opening Displacement (CMOD) was obtained from the numerical model, and Figure 9 represents the comparison between the numerical model and the experimental Force-CMOD curve, where a good accordance between two curves is noticed.

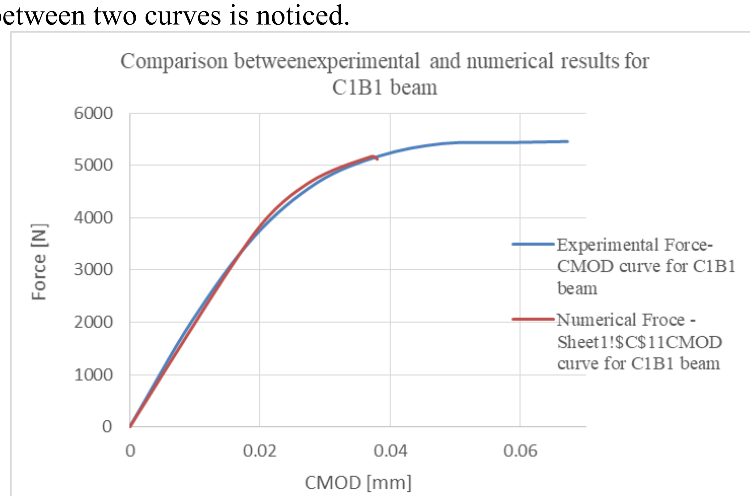

Figure 10. Comparison between the numerical and experimental Force-CMOD curve.

6 CONCLUSION

In the present study, the fracture behavior of a notched concrete beam in three points bending test was verified analytically, experimentally and numerically. Anew analytical model for predicting Force-Crack Mouth Opening Displacement (F-CMOD) for bending beam was proposed depending on the trilinear softening curve. This model solves the larger maximum force problem faced in bilinear softening based model. The parameters of the softening curve were found through the proposed model by minimizing the differences between the experimental F-CMOD curve obtained from three-point bending test on notched beams and the numerical one calculated from the model by means of regression. A normalized trilinear softening curve was introduced depending on 36 specimens from the present study and literature, using the material properties of concrete.

A three-point bending beam was modeled in ABAQUS using the extended finite element method (XFEM) approach. The beam was modeled using FEM, while the cracking zone was modelled using XFEM.

The numerical simulation gave results using XFEM approach which were close to the experimental ones.

REFERENCES

[ABAQUS 6.14] Abaqus Unified FEA, ABAQUS 6.14,(n.d.).https://www.3ds.com/fr/produits-etservices/simulia/produits/abaqus/.

[ASTM C33] ASTM Standard C33, 2003,“Specification for Concrete Aggregates,” ASTM International, West Conshohocken, PA, 2003, DOI: 10.1520/C0033-03.

[ASTM C150] ASTM C150/C150M, 2019, Standard Specification for Portland Cement, ASTM International.

[ASTM C192] ASTM C192/C192M, 2019, Standard Practice for Making and Curing Concrete Test Specimens in the Laboratory, ASTM International.

[ASTM C618] ASTM C618, 2019, Standard Specification for Coal Fly Ash and Raw or Calcined Natural Pozzolan for Use in Concrete, ASTM International.”

[Belytschko & Black 1999] Belytschko, T. Black, T. Elastic crack growth in finite elements with minimal remeshing, Int. J. Numer. Methods Eng. 45 (1999) 601–620.

[Brinker & Dahl 1989] Brinker R, Dahl H. "Fictitious crack model of concrete fracture". Magazine of Concrete Researches, 1989;41(147):79–86.

[Casuccio et al. 2008] Casuccio, M.,Torrijos, M.C, Giacio, G. Zerbino, R.(2008). "Failure mechanism of recycled aggregate concrete". Construction and Building Materials, 22(7): p. 1500-1506.

[CEB-FIP 90] Béton, C.E.-I.d., CEB-FIP Model Code 1990. 1990, Thomas Telford: London, UK. p. 437.

[Danhash *et al.* 2014 a] Danhash, G. Kousa, M. Wardeh, G. (2014), "Comparison between bilinear and power law softening curve of concrete using inverse analysis". 8th International Conference Analytical models in Concrete and Masonry Structures in Poland 16-18 June.

[Danhash *et al.* 2014 b] Danhash, G. Kousa, M. Wardeh, G. (2014), "The effect of paste volume and concrete properties on size independent fracture energy". Journal of Materials and Engineering Structures JMES 1, 58-72.

[Einsfeld *et al.* 2006] Einsfeld, R.A. and M.S.L. Velasco, (2006). "Fracture parameters for high-performance concrete". Cement and Concrete Research, 36(3): p. 576-583.

[50-FMC] 50-FMC Draft Recommendation, 1985- Determination of the fracture energy of mortar and concrete by means of three-point bend tests on notched beams. Materials and Structures/Matéiaux et Constructions,. 18(4): p. 287-290.

[Hillerborg *et al.* 1976] Hillerborg, A., M. Modéer, and P.-E. Petersson, 1976 -Analysis of crack formation and crack growth in concrete by means of fracture mechanics and finite elements. Cement and Concrete Research,. 6(6): p. 773-781.

[Karihaloo & Nallathambi 1991] Karihaloo, B.L. and P. Nallathambi, 1991- Notched beams test: model I fracture toughness, in Fracture Mechanics Test Method for concrete, S. Shah and A. Carpinteri, Editors. Chapmann& Hall. p. chapter 1, pages 1-86.

[KMIECIK & KAMIŃSKI 2011] KMIECIK, P. KAMIŃSKI, M. Modelling of reinforced concrete structures and composite structures with concrete strength degradation taken into consideration, Arch. Civ. Mech. Eng. 11 (2011) 623–636. Cement Concrete Compos;29(4):300–12.

[Melenk & Babuska 1996] Melenk, J.M. Babuska, I. The partition of unity finite element method: basic theory and applications, Comp. Meth. Appl. Mech. Eng. 39 (1996) 289–314.

[Olesen 2001] Olesen, J.F., Fictitious Crack Propagation in Fiber-Reinforced Concrete Beams. Journal of Engineering Mechanics, 2001. 127(3): p. 272-280.

[Ostergaard *et al.* 2003] Ostergaard, L., 2003- Early-Age Fracture Mechanics And Cracking of Concrete. Experiments and Modeling, in Department of Civil Engineering., Technical University of Denmark. p. 299.

[Roseler et al. 2007] Roesler J, Paulino GH, Park K, Gaedicke C. (2007). "Concrete fracture prediction using bilinear softening".

[Stang 2000] Stang, H., 2000- Analysis of 3 points bending test, Technical Report EU Contract - BRPR - CT98 - 813, Report from Test and Design Methods for Steel Fiber Reinforced concrete. p. 7.

[Ulfkjaer *et al.* 1995] Ulfkjaer, J.P., S. Krenk, and R. Brincker, 1995- Analytical Model for Fictitious Crack Propagation in Concrete Beams. Journal of Engineering Mechanics,. 121(1): p. 7-15.

[Wittmann *et al.* 1988] Wittmann, F., Rokugo, J. Bruwhiler, E. 1988- Fracture energy and strain softening of concrete as determined by means of compact tension specimens, in Materials and Structures., Springer Netherlands. p. 21-32.

[Zhang et al 2010] Zhang, J. Leung, C. Xu, S. (2010). "Evaluation of fracture parameters of concrete from bending test using inverse analysis approach", Materials and Structures, Springer Netherlands. p. 857-874.

[Zhao *et al.* 2008] Zhao, Z., Kwon, S.H. Shah, S.P. (2008). "Effect of specimen size on fracture energy and softening curve of concrete" Part I. Cement and Concrete Research. 38(8-9): p. 1049-1060.